TÜBİTAK

Turkish Journal of Earth Sciences

http://journals.tubitak.gov.tr/earth/

Research Article

Turkish J Earth Sci (2022) 31: 247-259

doi:10.55730/1300-0985.1771

Wide-area ground deformation monitoring in geothermal fields in western Turkey

Gökhan ASLAN[1,*], Hakkı AYDIN[2], Ziyadin ÇAKIR[3]

[1]Geological Survey of Norway (NGU), Trondheim, Norway

[2]Department of Petroleum and Natural Gas Engineering, Middle East Technical University, Ankara, Turkey

[3]Department of Geological Engineering, Faculty of Mines, İstanbul Technical University, İstanbul, Turkey

Received: 26.01.2022 • **Accepted/Published Online:** 19.04.2022 • **Final Version:** 18.05.2022

Abstract: The large-scale production and injection of geothermal fluids induce pressure, volume, and temperature gradient changes in the subsurface, which may result in surface deformation as well. Interferometric synthetic aperture radar (InSAR) is a promising utility for monitoring ground surface deformation and inferring subsurface reservoir operations that are difficult to observe directly. This study provides the first wide-area InSAR-derived long-term ground deformation across major geothermal fields in western Turkey. It aims to identify ground deformation hotspots within the geothermal exploitation sites and analyze their relationship with energy production and pumping. In the present study, the whole 2014–2020 Sentinel 1-A and 1-B SAR archive available over the region along ascending and descending orbits was processed using the persistent scatterer interferometry (PS-InSAR) technique. Compaction and land subsidence hot spots caused by fluid withdrawal are found within the geothermal fields. The results indicate that the observed systematic surface subsidence deformation result from the increase of geothermal production during the observation period in western Turkey. The real-time power data of geothermal plants retrieved from the transparency platform of the Turkish energy exchange are related to surface deformation. We estimated the drainage area of the production wells using subsidence deformation, caused by pore pressure decline in the reservoir. The results provide supporting evidence for the systematic monitoring and identification of deformation patterns in spatial-temporal extend can reveal reservoir dynamics and compartments, which are crucial for reservoir characterization and field development plan.

Key words: InSAR, geothermal, Sentinel, Germencik, Kızıldere, Alaşehir

1. Introduction

In general, geothermal systems are dominated either by a convection (viable or active) or conduction (passive) heat transfer regimes. Convection-dominated geothermal systems occur adjacent to a region of active tectonism, active volcanism and extensional tectonics and structural controls play a major role on fluid flow pathways. In contrast, conduction-dominated geothermal systems are located predominantly at passive tectonic plates where no significant recent significant tectonism or volcanism occurs (Moeck, 2014). Geothermal fields have long been linked the presence of predominant subterranean fracture systems that are presumed to control the stratigraphic structure and provide pathways for the transport of hot fluids (Hammond and Kreemer, 2007). In most major geothermal areas worldwide, active faulting is one important way of forming and keeping open, permeable channels suitable for the circulation of geothermal fluids (Morgan and Daggett, 1980). Therefore, plate tectonics settings have a fundamental influence on the locations of geothermal energy resources.

Turkey is a country with abundant geothermal energy resources owing to its favourable geological condition and tectonic setting, particularly in its western regions. The country ranks fourth globally with 1613 MWe cumulative installed geothermal power capacity as of August 2021 (REN21). Turkey's energy policy relies on expanding renewable energy in a cost-effective manner enabling energy diversity, which is critical for energy security. Turkey's Eleventh Development Plan (2019–2023) involves increasing the share of renewable energy sources in electricity generation 30% by 2023 to improve its energy independence and energy security. In this sense, geothermal energy for power and heat generation has been gaining momentum with a significant installed capacity and numerous undergoing projects in recent years to achieve this goal.

Major geothermal reservoirs in Turkey consist from metamorphics, containing marble, quartzite, and schist with liquid dominated geothermal fluid including significant amount of noncondensable gases. Medium

* Correspondence: gokhan.aslan@ngu.no

to high-temperature geothermal fluid (150–250 °C) is utilized for electricity generation using flashing type and binary type power plants. Noncondensable gas is released to the atmosphere while the waste brine is injected into reservoir for material balance and pressure maintenance in the reservoir. However, local pressure drop generally occurs due to pressure interferences between production wells. This cyclic procedure involves many thermal, hydrological, mechanical, and chemical processes (Liu et al., 2018) and can locally change pore pressure, temperature gradient, and volume around the well, which may yield some ground deformation. Since the energy per unit mass of geothermal water is relatively low compared to that of oil and coal, a huge volume of water is being extracted during geothermal energy production (Glowacka et al., 2005). A drastic volume of underground water extracted from the reservoir is partially compensated by a reduction of the volume of the reservoir. Such an immense fluid extraction process can also perturb the regional crustal stress field and induce earthquakes (Majer et al., 2007; Evans et al., 2012; Zang et al., 2014; Maurer et al., 2020) and hence surface deformation. Also, fluid extraction cools the reservoir causing thermal shrinkage and hence further volume reduction and deformation propagate to the ground surface (Glowacka et al., 2005). These surface deformations can negatively impact the underground and overground structures and operations of the geothermal reservoirs. In order to reduce the risk of production-induced ground deformation and other related effects such as induced seismicity, systematic and continuous monitoring of the surface deformation over the field is key information for the planning of future production strategies. Compared with the time-consuming and expensive ground-based conventional methods such as levelling and GPS measurements for mapping the ground deformation related to geothermal subsurface processes, InSAR technology allows for millimetric-precision measurements of wide-area ground deformation cost-effectively and continuously. The application of InSAR techniques using the different SAR sensors and processing approaches to image surface deformation associated with the operation of geothermal reservoirs has been well documented for almost last two decades (Massonnet et al., 1997; Carnec and Fabriol, 1999; Fialko and Simons, 2000; Vasco et al., 2002; Ali et al., 2016; Barbour et al., 2016; Juncu et al., 2017; Liu et al., 2018, Cigna et al., 2019). InSAR-derived surface displacement patterns have been also utilized to retrieve the three-dimensional spatial distribution of volumetric ground deformation sources such as subsurface fluid volume strain (Vasco et al., 2002) and source deep parameters (Fialko and Simons, 2000).

In the present study, we compute the time series of the ground deformation fields by combining the various multitrack InSAR datasets acquired by Copernicus Sentinel-1 satellite imaging over the geothermal fields in western Turkey (Figures 1 and 2).

2. Study area

The continental collision of the African and Eurasian plates dominates the active tectonics of the eastern Mediterranean (e.g., Jackson and McKenzie, 1984). This collision has induced collisional intercontinental convergence in Eastern Turkey and tectonic escape-related deformation in western Turkey, which is accommodated by right-lateral strike-slip North Anatolian Fault (NAF) to the north and left-lateral strike-slip East Anatolian Fault to the south-east of Turkey (see inset map in Figure 1; Şengör et al., 1985). To the south and west, the Anatolian plate is bounded by an active plate margin formed by the Hellenic and Cyprus trenches associated with back-arc spreading throughout Greece and western Turkey as African plate subducting northward (Westaway, 2013). As a result of such a wide variety of tectonic processes associated with African, Arabian, Eurasian and Anatolian plate interactions, an extension region has developed in the western Anatolia caused E–W- and NE–SW-trending graben structures where abundant geothermal activity is present (Frauds et al., 2010). The divergent and convergent plate boundaries are of great importance for the development of the geothermal systems in the region as they act as conduits for geothermal fluids. The heat from the shallow asthenospheric mantle is suggested to be transmitted toward the surface by fluid circulation along both the faults and faulting-induced fractures, and then accumulate within a suitable environment with high porosity, and so result in the reservoir of the geothermal system (Roche et al., 2005; Kocyigit, 2015). Hence, the presence of the fault system, their permeability, and their influence on the stratigraphic structure represents the first-order control on the heat transport and geothermal activity in the region (Roche et al., 2005; Faulds et al., 2006).

The Menderes Massif geothermal province is characterized by elevated heat flow values (approximately 100 mW m^{-2}) that extend to almost the entire Aegean domain (Erkan, 2014). The region includes the highest enthalpy geothermal systems found in Turkey localized along the margins of the deep grabens of the Menderes Massif (Serpen et al., 2009). These high temperatures are associated with the circulation of surface waters through deeply incised E-W striking normal faults in the Menderes horst-graben system (Erkan, 2014). Menderes metamorphics have conductive faults and fault-associated fractures, which are the primary flow paths for geothermal fluid in the reservoir. Menderes metamorphics consist of Paleozoic aged reservoir rock containing marble, mica-schist, calc-shist, and quartz. Reservoir fluid is the liquid-dominated and meteoric origin (Aydin and Akin,

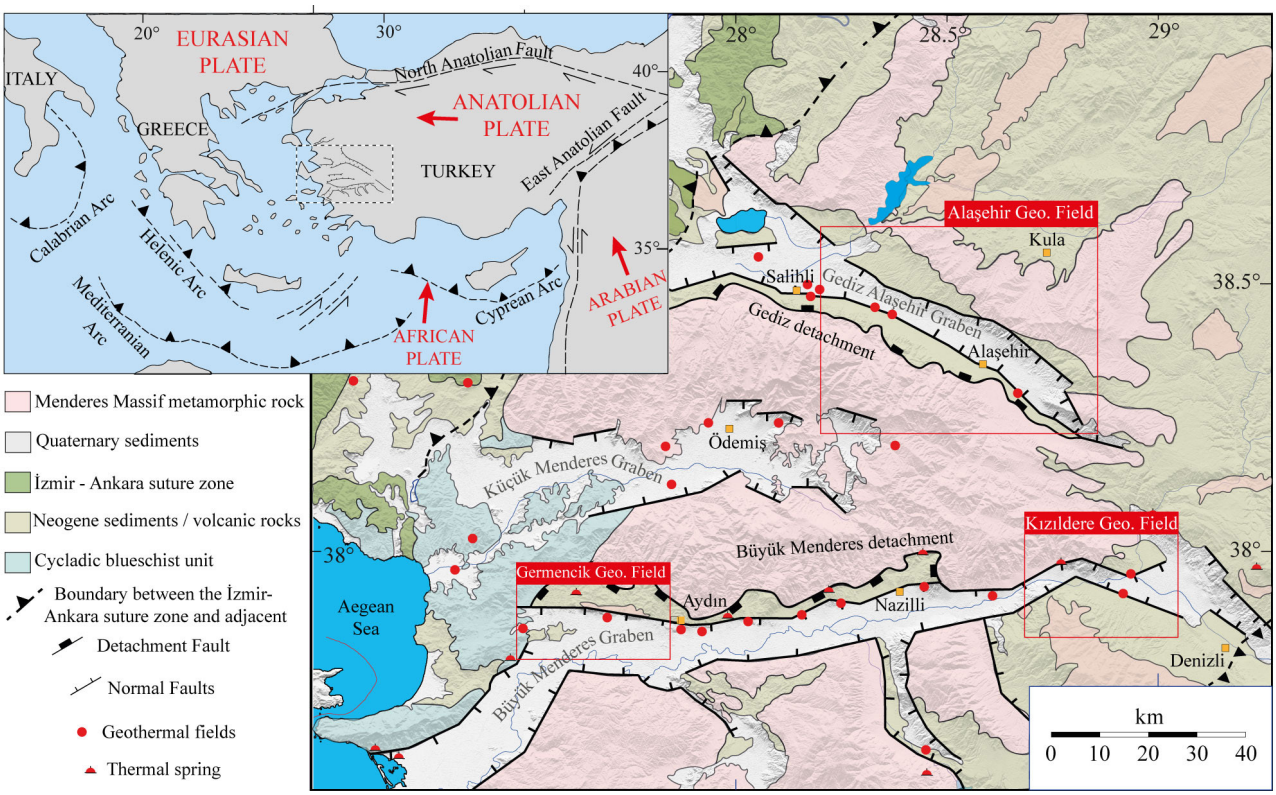

Figure 1. Geological map of western Turkey showing the Menderes Massif and its subdivision into the Gediz-Alaşehir graben (GAG), Küçük Menderes graben (KMG) and Büyük Menderes graben (BMG) overlain on shaded topography of 30-m spacing ALOS DEM data (mainly modified from Bozkurt, 2007 and Kaya, 2015). The inset map shows the tectonic setting of the Aegean and Eastern Mediterranean regions. The study area is outlined by the black dashed rectangle on the inset map. The red spheres and semispheres represent the locations of deep geothermal wells and hot springs, respectively (Karakus and Simsek, 2013).

2021). Various tectonic movements have resulted in the crustal thinning of western Anatolia. The active tectonic mechanism in western Anatolia created E-W trending normal faults, the main target for geothermal drilling wells. Production wells that target these faults provide large flow rates (100–500 tons per hour) with considerable reservoir temperatures (150–250 °C). More than 100 wells have been drilled in Alaşehir, Kızıldere, and Germencik fields. Huge fluid volumes have been produced from a limited area resulted in significant pressure drop locally. As a result of such pressure decline, the pore volume of the reservoir is reduced, which is monitored on the surface as ground deformation. In this study, we will mainly focus on the InSAR-derived ground deformation associated with geothermal activities along with the Alaşehir, Germencik, and Kızıldere geothermal fields in western Turkey (Figure 1).

3. InSAR data and methodology

3.1. InSAR Datasets

We used data from the European Space Agency Sentinel-1 SAR constellation, which is composed of two satellites that were launched in April 2014 (S1A) and April 2016 (S1B) and equipped with C-band SAR sensors. The Sentinel-1 operation in terrain observation with progressive scan (TOPS) mode represents an important advantage compared to other sensors' modes as it provides wide-area coverage and a short revisit time of up to 6-days over Europe and 12-days globally. Here, we processed SAR datasets acquired on four overlapping tracks in ascending (T131 and T58) and descending (T36, T138) orbits, consisting respectively of 280, 256, 262, and 278 images over the period of 2014–2020. We employed an individual set of interferograms for each track with a sufficiently high phase coherence pattern over the study area.

3.2. PS-InSAR processing

We computed all interferograms using the open-source software GMTSAR (Sandwell et al., 2011) based on a single reference network for persistent scatterer interferometry analysis. The choice of the reference images is made on the basis of having the most optimal spatial and temporal baselines for all the pairs of interferograms (Figure 3). To compute the simulation of the topographic phase in the interferograms, we used the Shuttle Radar Topography

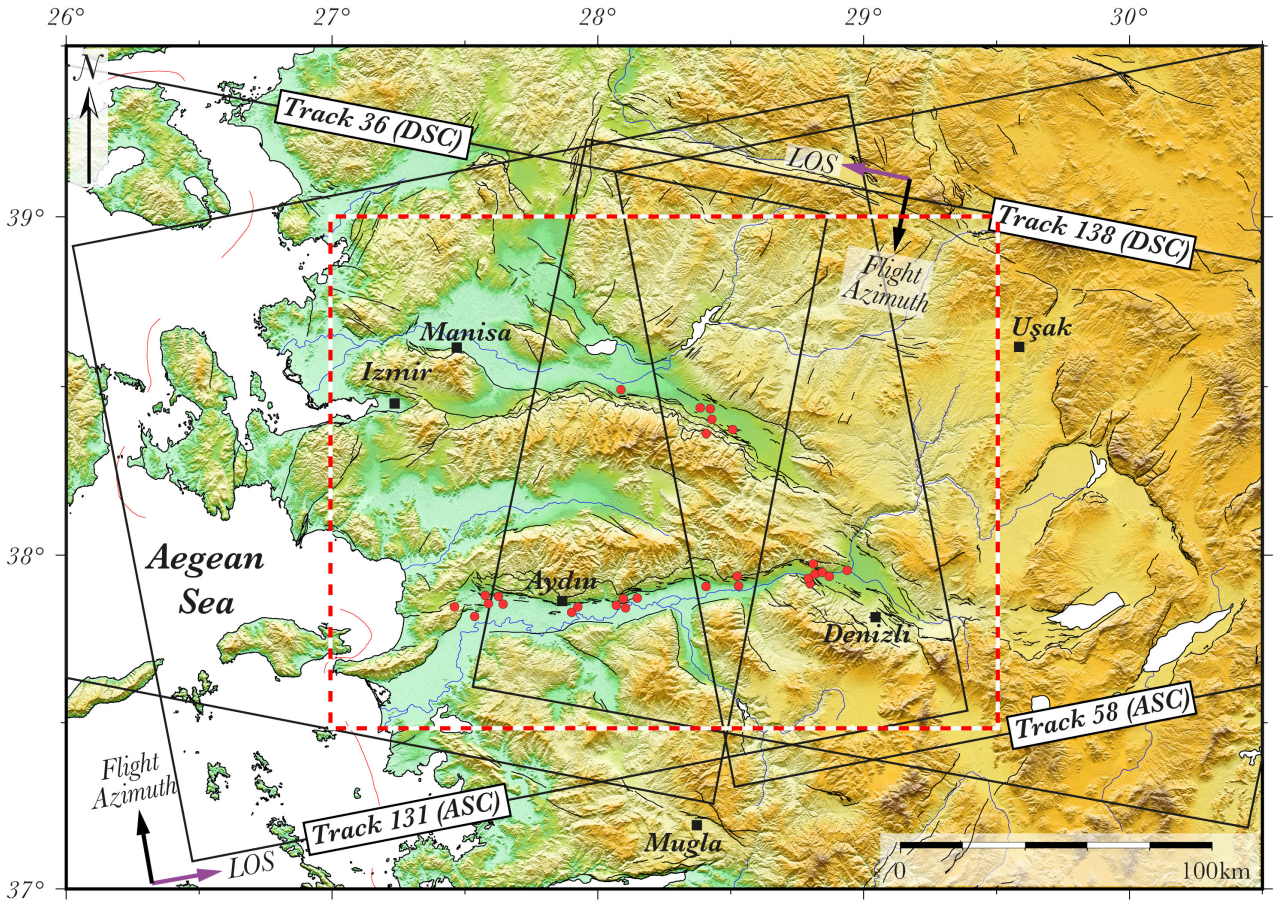

Figure 2. Study area and SAR data coverage overlain on the 30-m shaded topography (ALOS AW3D30 DEM data). The study area is outlined by the red-white dashed rectangle. The black rectangles represent the coverage of the SAR data used in this study. Black lines denote the active fault lines surrounding (Emre et al., 2013). The locations of active geothermal power stations are marked as red dots along the graben systems.

Mission 3-arcsecond (approximately 90 m resolution) digital elevation model (Farr et al., 2007). We processed the single reference stacks of interferograms using the StaMPS software package (Hooper, 2008; Hooper et al., 2012), which allows the identification of PS points using both amplitude and phase information. In a first step, the initial PS points are selected based on their noise characteristics, using the amplitude dispersion criterion defined by $D_{amp} = \sigma_{Amp} / m_{Amp}$), where σ_{Amp} and m_{Amp} are the standard deviation and mean of the amplitude in time, respectively (Ferretti et al., 2001). We selected a threshold value of $D_{amp} = 0.34$ that minimizes the random amplitude variability and eliminates highly decorrelated pixels in some areas covered with vegetation, agricultural fields, or snow. After the selection of stable PS targets based on amplitude analysis, the PS probability is refined by phase analysis in a series of iterations. This process allows the detection of stable pixels even with low amplitude. Once the final selection of PSs has been done, the residual topographic component can be removed. Then, phase unwrapping is performed both spatially and temporally. This analysis enables retrieval of the average line-of-sight (LOS) surface deformation rate maps. To remove atmospheric effects from interferograms, we used the freely available Toolbox for Reducing Atmospheric InSAR Noise (Bekaert et al., 2015). This toolbox uses ERA-Interim (ERA-I, European Center for Medium-Range Weather Forecast) numerical weather model datasets (Dee et al., 2011).

3.3. Decomposition of Sentinel-1 data into 2D displacement rates

The subsidence signal over the study area is covered entirely by Sentinel-1 data from four different orbits. We decomposed the mean PS-InSAR line-of-sight velocity fields into east-west and vertical components by assuming that the north-south displacement was negligible because the near-polar orbits of the SAR satellites produce a low sensitivity to the north-south component of displacement (Wright et al., 2004). In a first step, we resampled the mean

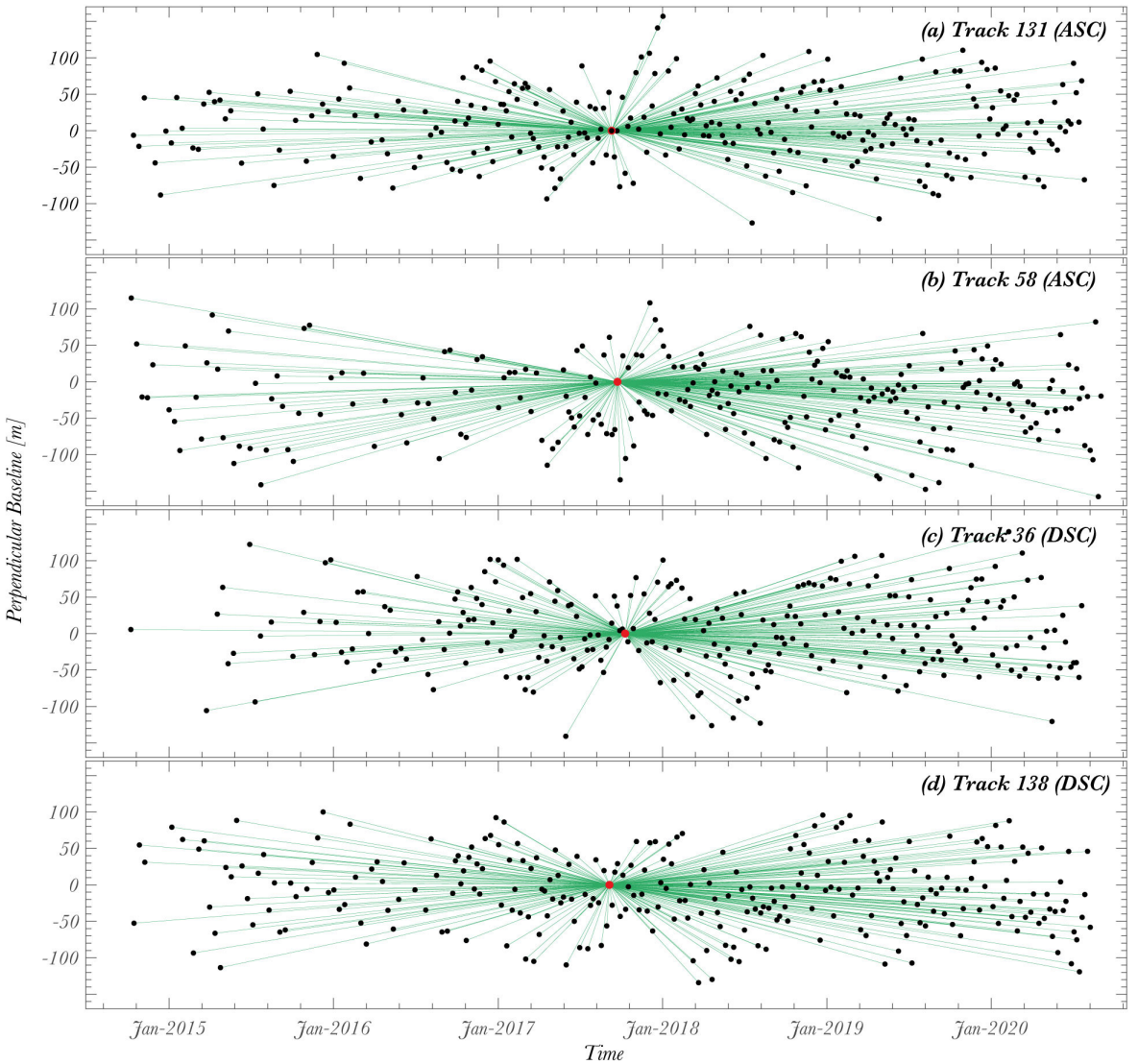

Figure 3. Plot of baseline versus acquisition date of SAR images for different Sentinel 1-A/B tracks used to compute displacement fields and time series. Black dots indicate SAR images, and red dot indicate the reference image chosen for time series analyses. Green lines connect pairs (interferograms).

line-of-sight velocities for the ascending and descending tracks onto a 100 × 100 m regular grid, which was used as input for displacement decomposition. We used the nearest-neighbor procedure to resample the persistent scatterer pixels that are within 200 m of the center of each grid nodal point. In a second step, we selected all the pixels that exist in both the ascending and descending tracks. Before decomposition, we transformed the InSAR mean velocity fields of both tracks into the same reference frame using a reference area deemed to be a geologically stable area. In the last step, the line-of-sight velocity fields were decomposed into two components: The horizontal component along the east-west direction (d_{hor}) and the vertical component (d_{ver}) were computed, considering the local incidence angle of the satellite view by solving the following equation (Motagh et al., 2017).

$$\begin{pmatrix} d_{asc} \\ d_{dsc} \end{pmatrix} = \begin{pmatrix} cos\theta_{asc} & -cos\alpha_{asc} \,.\, sin\theta_{asc} \\ cos\theta_{dsc} & -cos\alpha_{dsc} \,.\, sin\theta_{dsc} \end{pmatrix} \begin{pmatrix} d_{ver} \\ d_{hor} \end{pmatrix} \quad (1)$$

where θ_{asc} and θ_{dsc} represent the local incidence angles and a_{asc} and a_{dsc} are the satellite heading angles in the ascending and descending modes, respectively.

4. Results and discussion

4.1. Mean line-of-sight velocity fields

The region surveyed with multitemporal multitrack InSAR time-series analysis covers a total 36,000 km^2. Apparent spatial mean velocity deformation patterns indicating the

occurrence of ground deformation were observed within the Menderes graben system in the region (Figure 4). The areas with detected ground deformation are discussed in the following sections: focusing on the principal geothermal fields in the study area: Alaşehir, Germencik, and Kızıldere geothermal areas.

First of all, the favorable geological, hydraulic, and stress control on geothermal resources in relation to the local tectonic setting is described for each geothermal field that has been targeted for ground deformation monitoring. After that, the geothermal power facilities and the development of each field that begins with the drilling of sufficient production and reinjection wells to feed the plant are highlighted. Finally, the real-time power generation data of geothermal plants retrieved from the transparency platform of the Turkish energy exchange and the well-head pressure evolution are related to the InSAR-derived surface deformation.

Time series analysis of 1076 Sentinel IW SAR images on the four tracks reveals the spatio-temporal evolution of the subsidence signal within the graben systems. The region examined here is mostly covered by the Mediterranean macchia, scrubland vegetation forest type providing a favorable coherency for interferometric SAR processing except for the agricultural areas within the grabens marked by very low PS density. The calculated PS densities from the four different datasets over the entire area of interest are 300 points/km^2.

4.2. Germencik geothermal field

The Germencik geothermal field is located at the western of the Büyük Menderes Graben (see Figure 2) in Aydın. The Quaternary to Miocene-age sedimentary rocks that fill the graben are juxtaposed against the Paleozoic metamorphics of the Kızılcagedik Horst by the E-W trending, S-dipping, normal Ömerbeyli Fault that forms the northern boundary of the field. E-W trending and S-dipping listric faults are the major faults in the field. Quaternary alluvium covers the surface of the field with depths ranging from 50 to 150 m. Pleistocene to Miocene-age volcanogenic sediments are deposited with a thickness up to 1200 m. The Palaeozoic aged metamorphic consisting of schists, quartz, marbles, and Cal-schist are the main reservoir rock and the

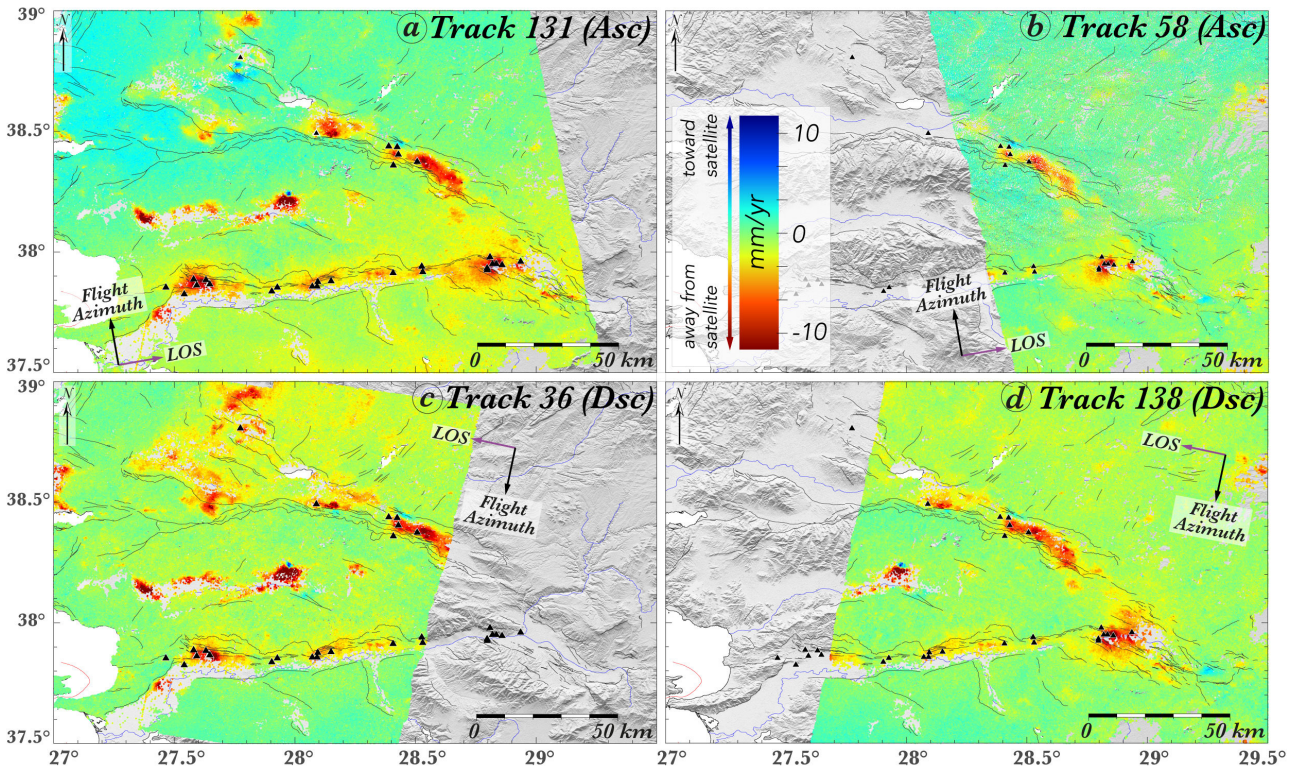

Figure 4. Results of the PS-InSAR time-series analysis for the area of interest in western Turkey, showing mean line-of-sight (LOS) velocity fields for the period 2014–2020 estimated from Sentinel 1A/B ascending tracks 131, 58 (a, b) and descending tracks 36, 138 (c, d). The positive velocities (cold colors) represent the motion of the ground toward the satellite and negative velocities (warm colors) represent motion away from the satellite. Purple and black arrows show line-of-sight and flight directions of the satellites, respectively. Locations of the 47 active geothermal power stations are marked as black triangles. The active faults (Emre et al., 2013) are drawn with thin black lines.

basement of the field. Akin (2018) defined two main producing sections, which are Vişneli formation (250–1000 m depth), and Menderes metamorphics (basement). The field was discovered by MTA (General Directorate of Mineral Research and Exploration) in 1968, and more than 38 wells have been drilled since then (Türeyen et al., 2014). The presence of hot springs, hydrothermal alterations, and shallow wells with hot water are indications of high heat flux intrusion in the region (Akin, 2018). The Germencik liquid-dominated field with high reservoir temperature up to 200-232 °C (Filiz et al., 2000) and the field has been actively operating with two 47.4 MWe dual flash and four 22.5 MWe binary power plants since 2009. As the spatial distribution of surface deformation in the Germencik field is analyzed, surface deformation is higher than 15 mm/year concentrated at the production region (Figure 5). The reinjection area has relatively lower deformations compared to the production region. There is a local pressure drop in the Germencik field, which means that pressure support from the reinjection side is insufficient for the production region. Surface deformation is at a constant rate and has not stabilized since 2015. The constant rate of surface deformation might be related to the commissioning of new power plants in the field. Surface deformation is found directly proportional to an increase in power capacity in the Germencik field (Figure 6).

4.3. Kızıldere geothermal field

The Kızıldere geothermal field is located on a positive fault block complex on the north flank of the Büyük Menderes Graben within the limits of Denizli Province (Dam and Erentöz, 1970). It is Turkey's first and high-potential geothermal field with high source temperature between 150 and 245 °C. The field is controlled by numerous faults and stratigraphic units. Gökdere, Gebeler, and East-West trending normal faults are important faults in the field. Most of the wells are concentrated on Gebeler faults, and newly drilled wells are targeting east-west trending normal faults at depths ranging from 3000 m to 4500 m depth. Menderes metamorphic is the basement and the main productive section of the field. The metamorphic are overlaid by Sazak formation, İğdecik formation, and fractured quartzite-calc-schist of the Metamorphic. The first geothermal power was installed in 1984. It is the first geothermal power plant in Turkey, a single flash type plant with a capacity of 17.4 MWe gross power. Shallow depth wells ranging from 400 m to 700 m feed the power plants with an average reservoir temperature of 190 °C. In 2013, a combined power plant, including a triple flash and a binary system, has 80 MWe power capacity. In 2017 and 2018, 165 MWe, another combined power plant, was commissioned in two units. More than 100 geothermal wells have been operated in the field. The high number of production wells created substantial changes in the reservoir dynamics. Şentürk et al. (2020) reported significant pressure drops in 2 years of production as new wells were put on the operation. In this study, we assess the ground deformation, which might be associated with the aforementioned reservoir pressure drop in the particular field area. Due to power plant technology (triple flash), 25%–30% of the produced fluid is released to the atmosphere through the wet cooling tower. Besides, there is vertical compartmentalization causing a weak hydraulic connection between shallow depth injection wells and deep production wells. Despite the injection rehabilitation program reported in Şentürk et al. (2020),

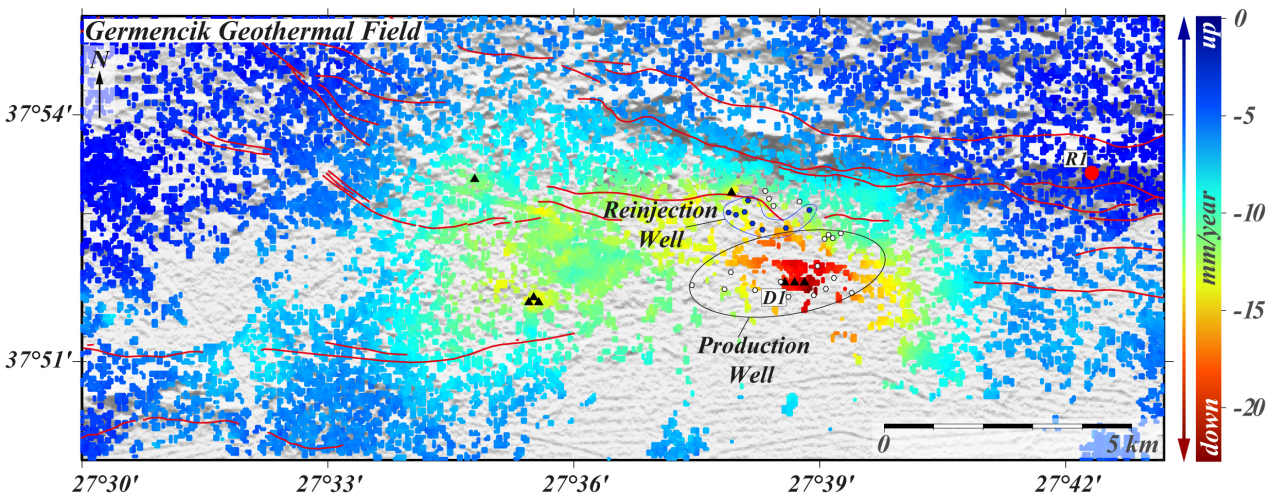

Figure 5. Spatial distribution of surface deformation in the Germencik geothermal field. The mean velocity value of the PS-InSAR points marked by the square of D1 is used to illustrate the temporal evolution of the subsidence (Figure 6) with respect to the reference PS points within the red point (R1) in the northeast region, which is considered to be a stable area.

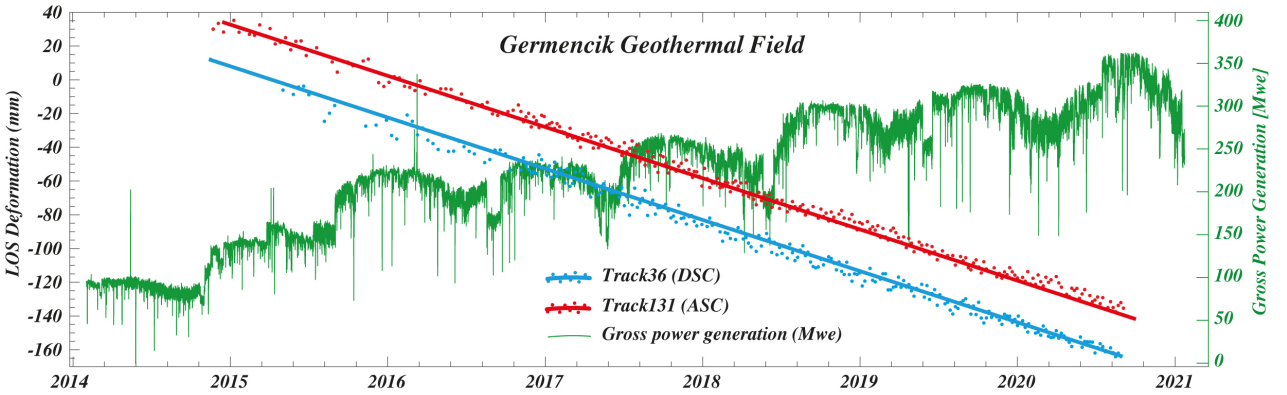

Figure 6. Evolution of surface deformation with respect to gross power generation in the Germencik geothermal field. InSAR time-series are shifted in order to better illustrate the consistency.

it seems that there is a continuous pressure decline in the reservoir, which can be found from surface deformation. The pressure decline in the field is in accordance with ground deformation. The maximum surface deformation is more than 15 mm per year, concentrated on the main producing fault, which is Gebeler fault (Figure 7). Using the surface deformation, the cumulative drainage area of the production wells is found as 5 km^2. By determining the drainage area from surface deformation, it is possible to identify new drilling locations, which will be less affected by existing production wells. As the surface deformation in the Kızıldere geothermal field is analyzed as a function of time, there is a time lag (6 months) between the starting dates of surface deformation and an increase in gross power generation. The discrepancy might be due to long-term production tests before the commissioning of power plants. Despite stabilization in power generation, the surface deformation continues at a constant rate (Figure 8). This means that there is a continuous decline in the reservoir pressure, which might be due to drilling make-up wells to stabilize power generation at a certain level.

4.4. Alaşehir geothermal field

The Alaşehir geothermal field is located in the south-eastern of Gediz-Alaşehir Graben that is controlled by two major normal fault systems. Alaşehir field is the most active geothermal field, which is operated by 7 different operators, operating 11 binary power plants and a combined geothermal plant. The installed power plants' capacity is 310 MWe from more than 100 wells, producing a total production rate of 12,600 tons per hour. Menderes metamorphic is the main producing section, consisting of marble, quartzite, and calc-schist. East-west trending and south-north trending normal faults are intersected, which provides large flow rates from 600 m to 3000 m depth reservoir. Aydin and Akin (2019) performed a discrete fracture network model in the field, reporting a pressure drop of 3 bar per year. Similar work was conducted by Aydin and Akin (2021), using a numerical reservoir simulation in the TOUGH2 reservoir simulator. Significant pressure drop and noncondensable gases decline was reported in both studies. Pressure decline in the reservoir might cause ground surface deformation. As the spatial distribution of surface deformation in the Alaşehir field is analyzed, the deformation is concentrated in two regions, where there are geothermal production wells (Figure 9). Comparatively, less deformation was observed in the reinjection area. We compared pressure decline with ground deformation in the field. It was found that there is a good correlation between pressure decline behavior, increase in power generation, and ground surface deformation in the Alaşehir field. As the wellhead flowing pressure was stabilized, the rate of surface deformation was decreased to a lower level (Figure 10).

Results report a slow and linear subsidence correlated with the geothermal production over the last six-year period. Geothermal wells have drainage areas determining by the volume of withdrawn fluid, reservoir fluid, and rock properties. The drainage area generally has a pressure decline behavior which eventually result in surface deformation because of pore volume variation at the reservoir level. Consequently, the drainage area of the production wells occupies an area of 60, 80, and 85 km^2 in the Kızıldere, Alaşehir, and Germencik fields, respectively. Thus, InSAR can be effectively used in terms of active data source during production and injection, providing crucial information about fluid flow paths, compartmentalization, and sweet spots for new drilling locations. As the time series are evaluated, it is apparent that pressure reduction in particular areas, dominating by local production is in good agreement with surface deformation.

5. Conclusion

High production rates from a limited geothermal area might cause surface deformation on the ground. Interferometric

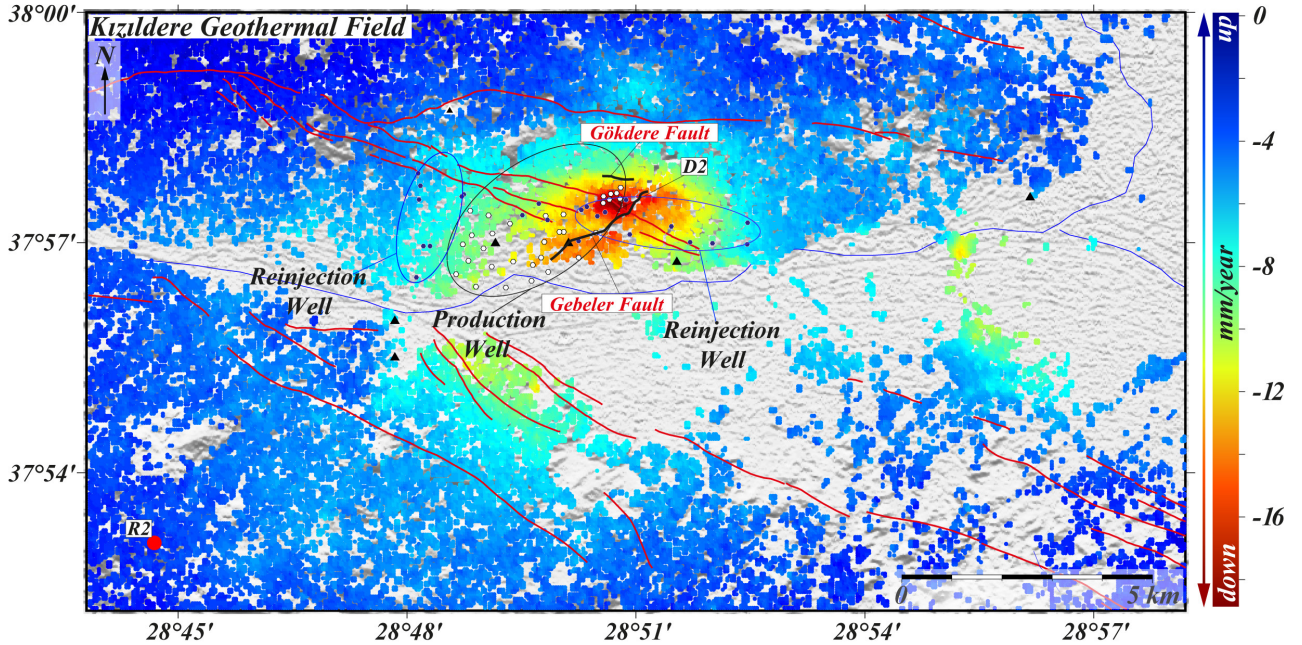

Figure 7. Spatial distribution of surface deformation in the Kızıldere geothermal field. The mean velocity value of the PS-InSAR points marked by the square of D2 is used to illustrate the temporal evolution of the subsidence (Figure 8) with respect to the reference PS points within the red point (R2) in the southwest region, which is considered to be a stable area.

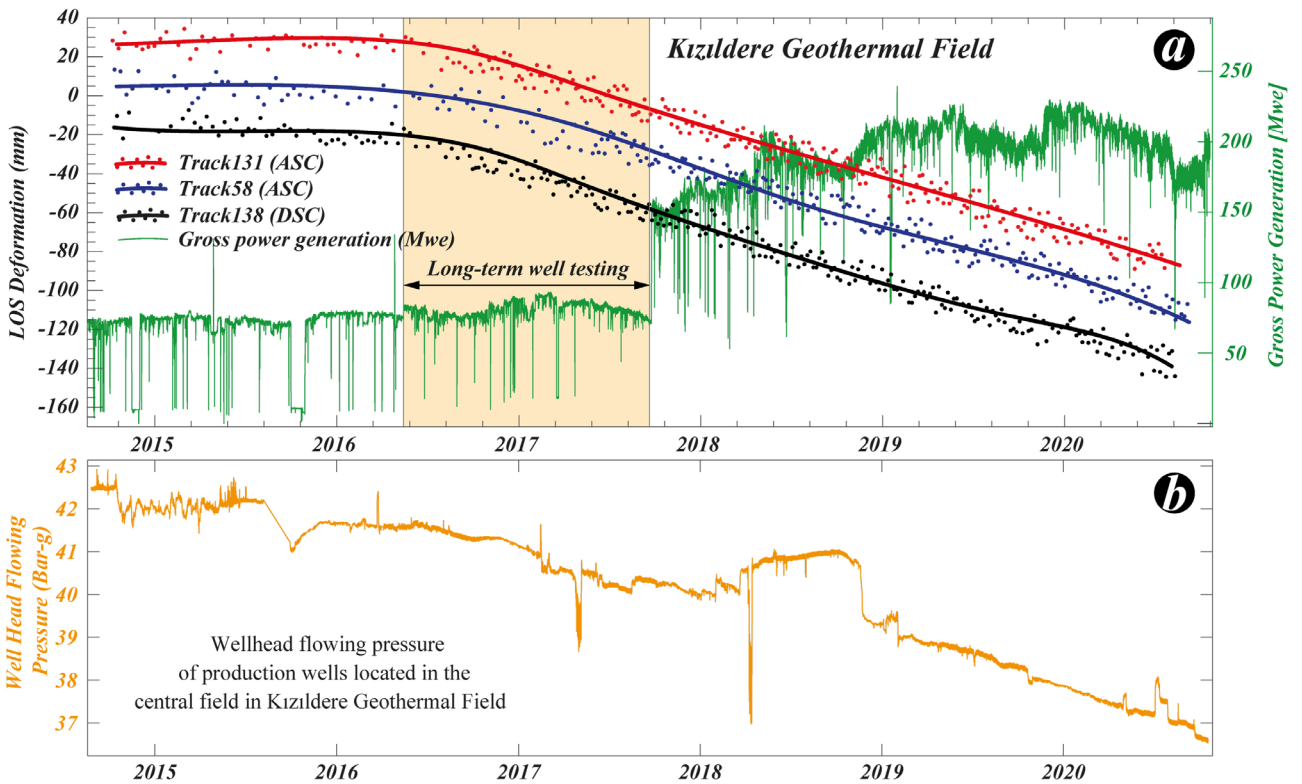

Figure 8. Evolution of surface deformation with respect to gross power generation and well-head flowing pressure in the Kızıldere geothermal field. InSAR time-series are shifted in order to better illustrate the consistency.

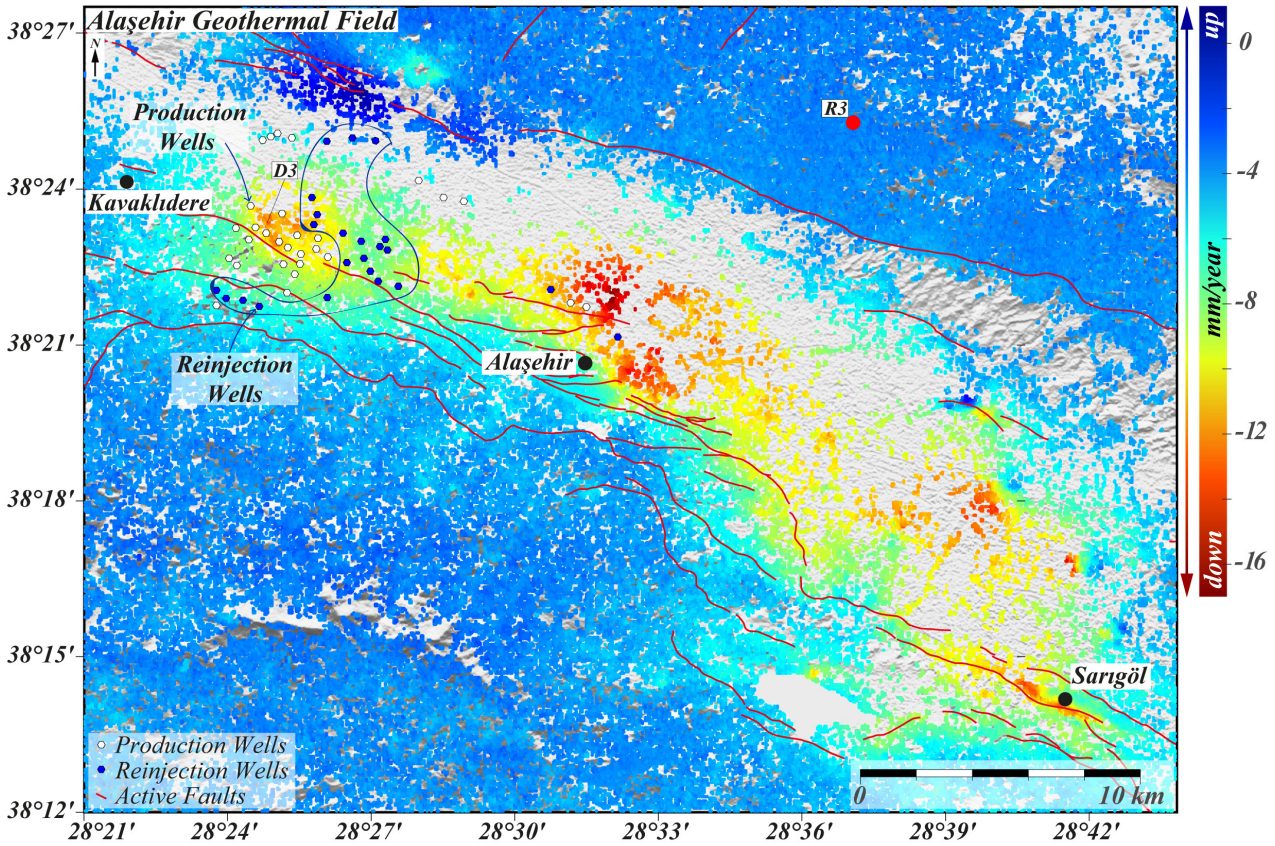

Figure 9. Spatial distribution of surface deformation in the Alaşehir geothermal field. The mean velocity value of the PS-InSAR points marked by the square of D3 is used to illustrate the temporal evolution of the subsidence (Figure 10) with respect to the reference PS points within the red point (R3) in the northeast region, which is considered to be a stable area.

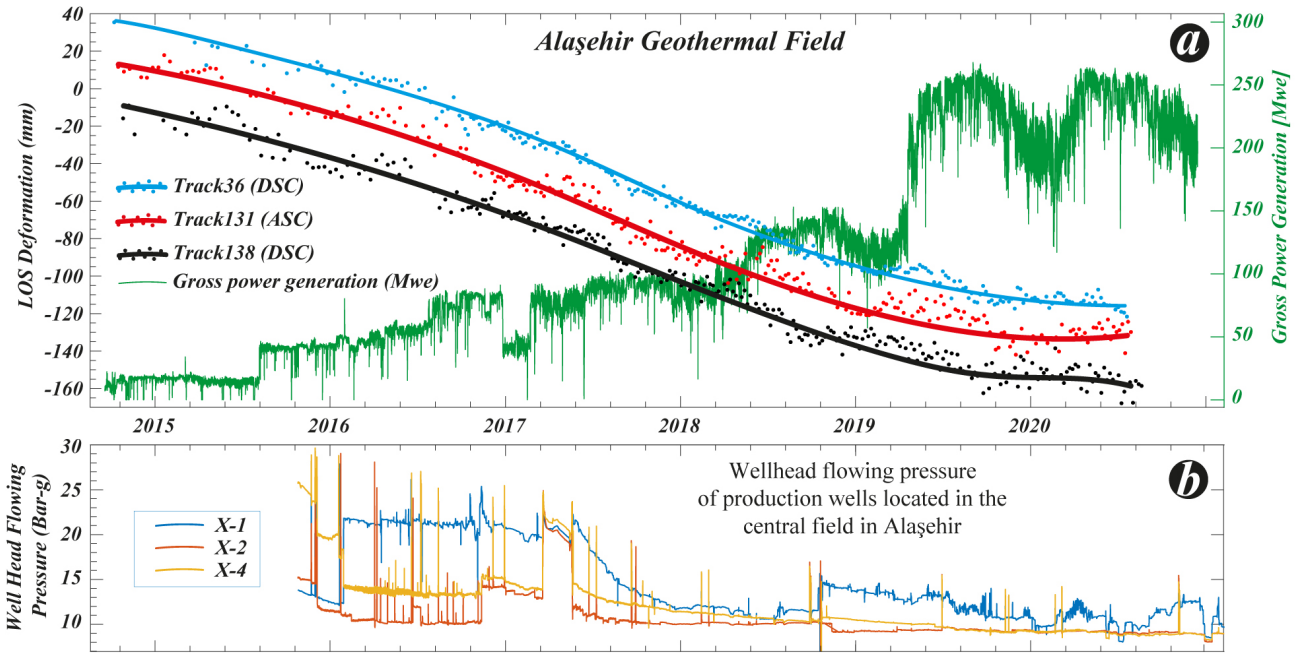

Figure 10. Evolution of surface deformation with respect to gross power generation and well-head flowing pressure in the Alaşehir geothermal field. InSAR time-series are shifted in order to better illustrate the consistency.

synthetic aperture radar (InSAR) is a promising utility for monitoring ground surface deformation and inferring subsurface reservoir operations that are difficult to observe directly. In this study, we evaluated surface deformation measured from major geothermal fields in western Anatolia: Germencik field, Kızıldere field, and Alaşehir field. Surface deformation measured from these fields was found directly proportional to the real-time power data of geothermal plants retrieved from the transparency platform of the Turkish energy exchange. As the spatial distribution of surface deformation in all the geothermal fields is analyzed, surface deformation of production regions is much higher than that of reinjection regions. This means that there is a local pressure drop in the fields. Measuring surface deformations in the geothermal areas are used to determine transient pressure regions that have experienced local pressure drops. Thus, the InSAR technique has been used as a strong tool for reservoir surveillance during long-term production. Depending on the aggressive production strategy and reservoir characteristics, the Germencik field and the Kızıldere field have shown surface deformation at a constant rate, while the surface deformation in the Alaşehir field is more stabilized. Strong hydraulic connections between injection and production wells in the Alaşehir field are in good agreement with this claim.

Acknowledgment
The raw interferometric products used in this study are freely distributed to the public via the European Space Agency (ESA) within the framework of the Copernicus Sentinel-1 mission (https://scihub.copernicus.eu/). Processing of Sentinel 1A/B images was performed at the Scientific and Technological Research Council of Turkey (TÜBİTAK) Turkish Academic Network and Information Center (ULAKBİM) and the High Performance and Grid Computing Center (TRUBA resources).

References

Ali ST, Akerley J, Baluyut, EC, Cardiff M, Davatzes NC et al. (2016). Time-series analysis of surface deformation at Brady Hot Springs geothermal field (Nevada) using interferometric synthetic aperture radar. Geothermics 61: 114-120. doi: 10.1016/j.geothermics.2016.01.008

Aydin H, Akin S (2021). Estimation of upcoming problems in Alaşehir geothermal field using a numerical reservoir model. Arabian Journal of Geosciences 14 (7): 1-20. doi: 10.1007/s12517-021-06830-z

Aydin H, Akin S (2019). Discrete Fracture Network Modeling of Alaşehir Geothermal Field. In: 44th Workshop on Geothermal Reservoir Engineering Stanford University; Stanford, California, United States. pp. 11-13.

Akin S (2018). Comprehensive Tracer Testing in the Germencik Field. In: 43rd Workshop on Geothermal Reservoir Engineering Stanford University; Stanford, California, United States

Barbour AJ, Evans EL, Hickman SH, Eneva M (2016). Subsidence rates at the southern Salton Sea consistent with reservoir depletion. Journal of Geophysical Research: Solid Earth 121(7): 5308-5327. doi: 10.1002/2016JB012903

Bekaert DPS, Walters RJ, Wright TJ, Hooper AJ, Parker DJ (2015). Statistical comparison of InSAR tropospheric correction techniques. Remote Sensing of Environment 170: 40-47. doi: 10.1016/j.rse.2015.08.035

Bozkurt E (2007). Extensional v. contractional origin for the southern Menderes shear zone, SW Turkey: tectonic and metamorphic implications. Geological Magazine 144(1): 191-210. doi: 10.1017/S0016756806002664

Carnec C, Fabriol H (1999). Monitoring and modeling land subsidence at the Cerro Prieto geothermal field, Baja California, Mexico, using SAR interferometry. Geophysical Research Letters 26(9): 1211-1214. doi: 10.1029/1999GL900062

Cigna F, Tapete D, Garduño-Monroy VH, Muñiz-Jauregui JA, García-Hernández OH et al. (2019). Wide-area InSAR survey of surface deformation in urban areas and geothermal fields in the eastern Trans-Mexican Volcanic Belt, Mexico. Remote Sensing 11(20): 2341. doi: 10.3390/rs11202341

Dee DP, Uppala SM, Simmons AJ, Berrisford P, Poli P et al. (2011). The ERA-Interim reanalysis: Configuration and performance of the data assimilation system. Quarterly Journal of the royal meteorological society 137(656): 553-597. doi: 10.1002/qj.828.

Erkan K (2014). Crustal heat flow measurements in western Anatolia from borehole equilibrium temperatures. Solid Earth Discuss 6: 403-426. doi: 10.5194/sed-6-403-2014

Evans KF, Zappone A, Kraft T, Deichmann N, Moia F (2012). A survey of the induced seismic responses to fluid injection in geothermal and CO2 reservoirs in Europe. Geothermics 41: 30-54. doi:10.1016/j.geothermics.2011.08.002

Emre O, Duman TY, Ozalp S, Elmaci H, Olgun S (2013). Active Fault Map of Turkey with and Explanatory Text, Ankara, Turkey, Special Publication Series-30. General Directorate of Mineral Research and Exploration, Ankara.

Farr TG, Rosen PA, Caro E, Crippen R, Duren R et al. (2007). The shuttle radar topography mission. Reviews of Geophysics 45(2): 25-36. doi: 10.1029/2005RG000183

Faulds J, Coolbaugh M, Bouchot V, Moek I, Oguz K (2010). Characterizing structural controls of geothermal reservoirs in the Great Basin, USA, and Western Turkey: developing successful exploration strategies in extended terranes. In: World Geothermal Congress; Bali, Indonesia. pp. 11-15.

Fialko Y, Simons M (2000). Deformation and seismicity in the Coso geothermal area, Inyo County, California: Observations and modeling using satellite radar interferometry. Journal of Geophysical Research: Solid Earth 105(B9): 21781-21793. doi: 10.1029/2000JB900169

Filiz S, Tarcan G, Gemici U (2000). Geochemistry of the Germencik geothermal fields, Turkey. In: Proceedings of the World Geothermal Congress; pp. 1115-1120.

Ferretti A, Prati C, Rocca F (2001). Permanent scatterers in SAR interferometry. IEEE Transactions on geoscience and remote sensing 39(1): 8-20. doi: 10.1109/36.898661

Glowacka E, Sarychikhina O, Nava FA (2005). Subsidence and stress change in the Cerro Prieto geothermal field, BC, Mexico. Pure and Applied Geophysics 162(11), 2095-2110. doi: 10.1007/s00024-005-2706-7

Haklidir FST, Şengül R, Aydin H (2021). Characterization and Comparison of geothermal fluids geochemistry within the Kızıldere Geothermal Field in Turkey: New findings with power capacity expanding studies. Geothermics 94 (2021): 102-110. doi: 10.1016/j.geothermics.2021.102110

Hooper A (2008). A multi-temporal InSAR method incorporating both persistent scatterer and small baseline approaches. Geophysical Research Letters 35(16). doi: 10.1029/2008GL034654.

Hooper A, Bekaert D, Spaans K, Arıkan M (2012). Recent advances in SAR interferometry time series analysis for measuring crustal deformation. Tectonophysics 514: 1-13. doi: 10.1016/j.tecto.2011.10.013.

Juncu D, Árnadóttir T, Hooper A, Gunnarsson G (2017). Anthropogenic and natural ground deformation in the Hengill geothermal area, Iceland. Journal of Geophysical Research: Solid Earth 122(1): 692-709. doi: 10.1002/2016JB013626

Jackson J, McKenzie D (1984). Active tectonics of the Alpine—Himalayan Belt between western Turkey and Pakistan. Geophysical Journal International 77(1): 185-264. doi: 10.1111/j.1365-246X.1984.tb01931.x

Jackson J, McKenzie D (1988). Rates of active deformation in the Aegean Sea and surrounding regions. Basin Research 1(3): 121-128. doi: 10.1111/j.1365-2117.1988.tb00009.x

Karakuş H, Şimşek Ş (2013). Tracing deep thermal water circulation systems in the E–W trending Büyük Menderes Graben, western Turkey. Journal of Volcanology and Geothermal Research 252: 38-52. doi: 10.1016/j.jvolgeores.2012.11.006

Kaya A (2015). The effects of extensional structures on the heat transport mechanism: an example from the Ortakçı geothermal field (Büyük Menderes Graben, SW Turkey). Journal of African Earth Sciences 108: 74-88. doi:10.1016/j.jafrearsci.2015.05.002

Koçyiğit A (2015). An overview on the main stratigraphic and structural features of a geothermal area: the case of Nazilli-Buharkent section of the Büyük Menderes Graben, SW Turkey. Geodinamica Acta 27(2-3): 85-109. doi: 10.1080/09853111.2014.957501

Liu F, Fu P, Mellors RJ, Plummer MA, Ali ST et al. (2018). Inferring Geothermal Reservoir Processes at the Raft River Geothermal Field, Idaho, USA, Through Modeling InSAR-Measured Surface Deformation. Journal of Geophysical Research: Solid Earth 123(5): 3645-3666, doi: 10.1029/2017JB015223

Massonnet D, Holzer T, Vadon H (1997). Land subsidence caused by the East Mesa geothermal field, California, observed using SAR interferometry. Geophysical Research Letters 24(8): 901-904. doi: 10.1029/97GL00817

Maurer V, Gaucher E, Grunberg M, Koepke R, Pestourie R et al (2020). Seismicity induced during the development of the Rittershoffen geothermal field, France. Geothermal Energy 8(1): 1-31. doi: 10.1186/s40517-020-0155-2

Majer EL, Baria R, Stark M, Oates S, Bommer J et al. (2007). Induced seismicity associated with enhanced geothermal systems. Geothermics 36(3): 185-222. doi: 10.1016/j.geothermics.2007.03.003

Moeck IS (2014). Catalog of geothermal play types based on geologic controls. Renewable and Sustainable Energy Reviews 37: 867-882. doi: 10.1016/j.rser.2014.05.032.

Morgan P, Daggett PH (1980). Active and passive seismic studies of geothermal resources in New Mexico and investigations of earthquake hazards to geothermal development, New Mexico State University, Las Cruces, New Mexico, United States.

Motagh M, Shamshiri R, Haghighi MH, Wetzel HU, Akbari B et al. (2017). Quantifying groundwater exploitation induced subsidence in the Rafsanjan plain, southeastern Iran, using InSAR time-series and in situ measurements. Engineering Geology 218: 134-151. doi: 10.1016/j.enggeo.2017.01.011

REN21 (2020). Renewables 2020 Global Status Report (ISBN 978-3-948393-00-7)

Roche V, Bouchot V, Beccaletto L, Jolivet L, Guillou-Frottier L et al. (2019). Structural, lithological, and geodynamic controls on geothermal activity in the Menderes geothermal Province (Western Anatolia, Turkey). International Journal of Earth Sciences 108(1): 301-328. doi: 10.1016/j.enggeo.2017.01.011

Sandwell D, Mellors R, Tong X, Wei M, Wessel P (2011). Open radar interferometry software for mapping surface deformation. Eos, Transactions American Geophysical Union 92(28): 234-234. doi: 10.1029/2011EO280002

Samieie-Esfahany S, Hanssen R, van Thienen-Visser K, Muntendam-Bos A (2009). On the effect of horizontal deformation on InSAR subsidence estimates. In: Proceedings of the Fringe 2009 Workshop, Frascati, Italy.

Serpen U, Aksoy N, Öngür T, Korkmaz ED (2009). Geothermal energy in Turkey: 2008 update. Geothermics 38(2): 227-237. doi: 10.1016/j.geothermics.2009.01.002

Senturk E, Aydin H, Tuzen MK (2020). Injection Rehabilitation at Kızıldere Geothermal Field: Use of Flow Rate Weighted Average Production Wellhead Pressure for Reservoir Management. In: 45th Workshop on Geothermal Reservoir Engineering, Stanford University; Stanford, California, United States.

Şengör AMC, Görür N, Şaroğlu F (1985). Strike-slip faulting and related basin formation in zones of tectonic escape: Turkey as a case study, Special Publications of SEPM

Tureyen OI, Sarak H, Gulgor A, Erkan B, Satman A (2014). A study on the production and reservoir performance of the Germencik geothermal field. In: Proceedings of the Thirty-Ninth Workshop on Geothermal Reservoir Engineering; pp. 24-26.

Ten-Dam A, Erentöz C (1970). Kızıldere geothermal field - Western Anatolia. Geothermics 2: 124-129.

The Presidency of the Republic of Turkey, Directorate of Strategy and Budget (DSB) (2018). Special expertise commission reports, 11th. Development plan [online]. Website https://www.sbb.gov.tr/wp-content/uploads/2021/12/Eleventh_Development_Plan_2019-2023.pdf)

Vasco DW, Wicks C, Karasaki K, Marques O (2002). Geodetic imaging: reservoir monitoring using satellite interferometry. Geophysical Journal International 149(3): 555-571. doi:10.1046/j.1365-246X.2002.01569.x

Westaway R (2003). Kinematics of the Middle East and Eastern Mediterranean Updated. Turkish Journal of Earth Sciences 12(1).

Wallace K, Dunford T, Ralph M, Harvey W (2009). Aegean Steam: Germencik Dual Flash Plant. In: Proceedings of the GeoFund-IGA Geothermal Workshop; pp. 16-19.

Wright TJ, Parsons BE, Lu Z (2004). Toward mapping surface deformation in three dimensions using InSAR. Geophysical Research Letters 31(1). doi: 10.1029/2003GL018827

Zang A, Oye V, Jousset P, Deichmann N, Gritto R (2014). Analysis of induced seismicity in geothermal reservoirs–An overview. Geothermics 52: 6-21. doi: 10.1016/j.geothermics.2014.06.005